Modeling the Fluid Flow around Airfoils Using Conformal Mapping

Nitin R. Kapania, Katherine Terracciano, Shannon Taylor

August 29, 2008

Abstract

The modeling of fluid interactions around airfoils is difficult given the complicated, often non-symmetric geometries involved. The complex variable technique of conformal mapping is a useful intermediate step that allows for complicated airfoil flow problems to be solved as problems with simpler geometry. In this paper, we use the conformal mapping technique to model the fluid flow around the NACA 0012, 2215, and 4412 airfoils by using the Joukowsky transformation to link the flow solution for a cylinder to that of an airfoil. The flow around a cylinder was derived with the superposition of elementary potential flows using an inviscid, incompressible fluid model. Lift calculations as a function of angle of attack for each airfoil were obtained using the transformed flow solutions and fundamental theories of aerodynamics. These calculations are compared against lift calculations provided by the thin airfoil method. Lift calculations for the NACA 0012 airfoil match well with expected results, while there is a discrepancy at low angles of attack for the 2215 and 4412 airfoils.

Key Terms: NACA airfoil, conformal mapping, Joukowsky transformation, inviscid flow.

1 Introduction

In the field of fluid dynamics, an area of significant practical importance is the study of airfoils. An airfoil refers to the cross sectional shape of an object designed to generate lift when moving through a fluid. Fundamentally, an airfoil generates lift by diverting the motion of fluid flowing over its surface in a downward direction, resulting in an upward reaction force by Newton's third law [2]. While this is an acceptable qualitative way of looking at airfoils, understanding the design of applicable systems such as airplanes, helicopters, and wind turbines requires a quantitative method of analyzing fluid flow and lift.

Understanding lift at a higher level thus involves the physical modeling of the fluid flowing over an airfoil. While this physical modeling is obviously an area of interest to those studying introductory fluid dynamics, it is also a relevant field for students studying advanced mathematics. In particular, one common method of modeling the fluid flow around an airfoil requires an understanding of complex number mathematics. This method, known as conformal mapping, will be the main focus of this paper. Our paper is therefore geared towards students with an understanding of multivariable calculus who wish to develop their understanding of complex variable mathematics.

Conformal mapping is a mathematical technique in which complicated geometries can be transformed by a mapping function into simpler geometries which still preserve both the angles and orientation of the original geometry [4]. Using this technique, the fluid flow around the geometry of an airfoil can be analyzed as the flow around a cylinder whose symmetry simplifies the needed computations. Because the functions that define the fluid flow satisfy Laplace's equation, the conformal mapping method allows for lift calculations on the cylinder to be equated to those on the corresponding airfoil [5].

In this analysis, we focus on modeling the two-dimensional fluid flow around airfoils using the conformal mapping technique. We will first briefly describe how airfoils are characterized

geometrically. Next, we will describe the physical model we used to represent the inviscid, incompressible fluid flow around an airfoil, and explain the theory behind conformal mapping. We will then use the Joukowsky transformation, a specific application of conformal mapping, to link the solution for flow around a cylinder to the solution for flow around an airfoil. We will show how we used computational tools to implement this conformal mapping transformation to compute the fluid flow and lift around three NACA airfoils we chose to model. Finally, we will compare our lift calculations to similar calculations found using thin airfoil theory, another method of modeling airfoil aerodynamics. These results will be supplemented with a quantitative error analysis in an attempt to explain any discrepancies in the two models.

2 Characterizing Airfoils

Before we develop a model for the fluid flow around airfoils, it is important to define airfoils geometrically and to acquaint ourselves with the nomenclature with which they are characterized.

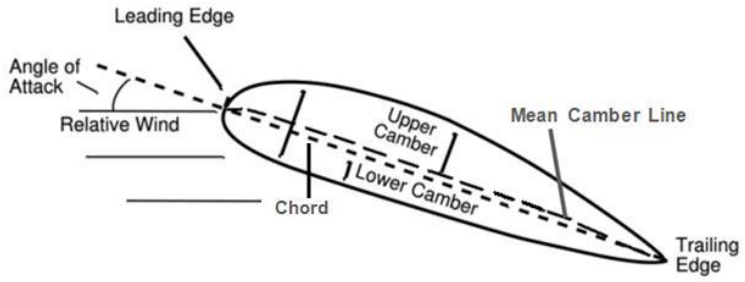

Figure 1: *Diagram of an airfoil with key parameters labeled.*[15]

The above diagram labels the main parameters of an airfoil that play a key role in its aerodynamic performance [15]. Specifically, we are interested in the angle of attack α, the chord length, and the mean camber line. The chord is a straight line typically used to

measure airfoil length, whereas the mean camber line is a curve halfway between the upper and lower surfaces used to measure airfoil curvature.

Airfoil shapes are commonly characterized with a numbering system originally defined by the National Advisory Committee for Aeronautics (NACA). This characterizing system defines airfoil shapes with a series of digits corresponding to non-dimensionalized airfoil properties. The number of digits used to describe an airfoil corresponds to the complexity of the airfoil. For this paper, we will only model four digit (4-series) airfoils to simplify the geometry of the airfoils we wish to analyze. In 4-series airfoils, the profile is defined as follows [1]:

1. The first digit describes the maximum camber as a percentage of the chord length. The maximum camber is the maximum distance between the chord and mean camber line along the axis of the chord.

2. The second digit indicates the position of the maximum camber in tenths of the chord.

3. The last two digits provide the maximum thickness of the airfoil as a percent of the chord length.

For example, a NACA 2412 airfoil would have a maximum camber that is 2% of the chord length, located 4/10 of the chord length away from the leading edge. This airfoil would have a maximum thickness that is 12% of the chord length.

3 Overview of Theories Used in Mathematical Modeling

3.1 Modeling Fluid Interactions with Inviscid Flow Theory

The modeling of fluid interactions around an airfoil is often divided into two branches [3]. One branch models the fluid around an airfoil as a real, viscous fluid. Since every fluid has some

viscosity, this branch is more accurate, but involves a degree of physical and mathematical complexity that goes beyond the scope of this paper. Instead, we use the second branch, and model the theoretical flow around an airfoil by treating the surrounding fluid as a "perfect fluid." These perfect fluids that we will model are considered inviscid, meaning they have no viscosity, and are incompressible, meaning their density remains constant. In reality, such perfect fluids do not exist, but considering the fluid flow as inviscid and incompressible still allows for an accurate model provided certain conditions are met [3].

The first of these conditions is that the airfoil must be moving through the fluid at subsonic speeds. This is important because at speeds approaching the speed of sound, shock waves occur in which the fluid flow no longer becomes continuous, and the perfect fluid idealization breaks down [7]. Specifically, our models will focus on airfoils moving through flow regions between Mach 0.0 and 0.4, as this is the range where compressibility effects in the fluid flow can be considered negligible.

The second assumption is that the flow over the airfoil satisfies the Kutta condition (see Fig. 2). The Kutta condition states that the fluid flowing over the upper and lower surfaces of the airfoil meets at the trailing edge of the airfoil [3]. This condition explains how an inviscid fluid can generate lift. In reality, it is friction between the boundary of an airfoil and the fluid that allows for the flow to meet smoothly at the trailing edge. Thus, the Kutta condition accounts for the friction at the boundary of an airfoil that is necessary for lift to be generated.

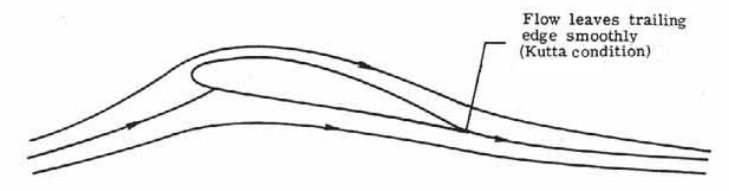

Figure 2: *Inviscid flow over an airfoil with the Kutta condition applied. Note how the flow meets smoothly at the trailing edge.* [15]

The Kutta condition forces two additional constraints on the flow around an airfoil. Firstly, the condition imposes that the leading and trailing edges of the airfoil are stagnation points where the fluid velocity vanishes [3]. Secondly, the angle of attack of the airfoil under consideration must remain well below a critical angle known as the stall angle. As the angle of attack increases beyond the stall angle, the Kutta condition is no longer physically applicable because the flow around an airfoil is no longer smooth and continuous.

3.2 Governing Equations for Inviscid Flow Theory

Having established the simplifications we will use to model the fluid flow around an airfoil, we now develop the governing equations that must be satisfied. Since we are considering our fluid to be perfectly incompressible, the density ρ of the fluid is constant. This means that for any fluid element with a given mass, the volume of that mass must remain constant. The principle of the conservation of mass is expressed for an incompressible flow by the equation

$$\nabla \cdot \vec{V} = 0 \tag{1}$$

Eq. 1 shows that for an incompressible fluid, the divergence of the velocity field $\vec{V}$ at every point must be 0. In addition, the lack of frictional shear forces acting on elements of an inviscid fluid causes the motion of the fluid to be purely translational, allowing the flow over an airfoil to be modeled as irrotational [3]. An irrotational flow is defined as a flow where the vorticity $\vec{\omega}$ is zero at every point. Since vorticity is defined as the curl of the velocity field, this imposes the condition

$$\vec{\omega} = \nabla \times \vec{V} = \vec{0} \tag{2}$$

If the velocity field $\vec{V}$ can be expressed as the gradient of a scalar potential function ϕ, such that $\vec{V} = \nabla\phi$, we have the relation

$$\nabla \times (\nabla \phi) = \vec{0} \tag{3}$$

Eq. 3 is true because by identity the curl of the gradient of a scalar function is 0. Eq. 3 demonstrates that for an irrotational flow, there exists a scalar function ϕ such that the velocity field of the flow is given by $\nabla \phi$. We therefore refer to ϕ as the velocity potential, and to flows that result from a velocity potential as potential flows.

Plugging in $\nabla \phi$ into Eq. 1 thus yields the final critical mathematical condition

$$\nabla \cdot (\nabla \phi) = \nabla^2 \phi = 0 \tag{4}$$

Eq. 4, also known as Laplace's equation, is extensively studied in mathematical physics. Solutions to this equation are referred to as harmonic functions, which are used to model the irrotational, incompressible fluid flow around airfoils. Since Laplace's equation is a linear second order partial differential equation, the sum of particular solutions to the differential equation is also a solution [3].

This means that, from a scalar velocity potential, we can also compute the stream function Ψ of a flow solution. The streamlines of the flow are visualized by setting the stream function Ψ equal to a constant. The relation between the velocity potential ϕ and the stream function Ψ is given by the equations

$$-\frac{\partial \Psi}{\partial x} = \frac{\partial \phi}{\partial y} \tag{5}$$

$$\frac{\partial \Psi}{\partial y} = -\frac{\partial \phi}{\partial x} \tag{6}$$

Eq's. 5 and 6, known as the Cauchy-Riemann relations, show that the stream lines given by the stream function and the equipotential curves given by the velocity potential are always

perpendicular. This is an important relation that makes conformal mapping a viable option for transforming potential flows.

3.3 The Conformal Mapping Technique

As Section 2 indicates, airfoils have complicated, often non-symmetric geometries. This makes it difficult to directly solve for the fluid flow around the airfoils using Laplace's equation and potential flow theory. To simplify the problem, the conformal mapping technique is used to extend the application of potential flow theory to practical aerodynamics [16].

A conformal map is the transformation of a complex valued function from one coordinate system to another. This is accomplished by means of a transformation function that is applied to the original complex function [4]. For example, consider a complex plane z shown in Fig. 3(a). Coordinates in this plane are defined with the complex function $z{=}x{+}iy$. This figure shows a simple uniform fluid flow with horizontal streamlines given by $\Psi = iy$ and equipotential curves given by $\phi = x$.

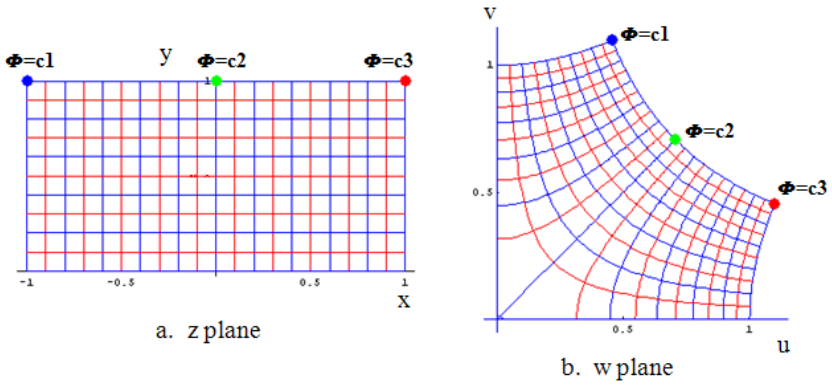

Figure 3: *A conformal mapping of a uniform flow with the transfer function* $w(z) = \sqrt{z}$. *The vertical lines in (a) represent equipotential curves, the horizontal lines represent stream lines. In (b), the conformal map maintains the perpendicular angle relationship between the streamlines and equipotential curves.*[10]

A conformal mapping can be used to transform this complex plane z into a new complex

plane given by $w = f(z)$, where in Fig. 3(b) $f(z)$ is the transformation function $w = \sqrt{z}$. The variables x and y in the z plane have been transformed to the new variables u and v. Note that while this transformation has changed the relative shape of the streamlines and equipotential curves, the set of curves remain perpendicular. This angle preserving feature is the essential component of conformal mapping. Because the relative orientation of the streamlines and potential curves remains the same, it can be proven that if a function is harmonic in the z plane, it is also harmonic in the transformed w plane [4]. As we will show in the next section, the flow around an airfoil shape can be developed by first solving for the flow around a cylinder in the z plane, and then transforming this solution to an airfoil in the w plane using a specific conformal mapping function.

4 Model of Fluid Flow around an Airfoil

4.1 Specific Solution to Fluid Flow around Cylinder

The first step to modeling the fluid flow around an airfoil is solving for the lifting flow around a cylinder in the z plane. This lifting flow can be modeled with the superposition of three basic, elementary flows. Because the solution for the flow around a cylinder has been studied extensively and is a staple of many aerodynamic textbooks, we will not delve in the specifics of the solutions in this paper.

4.1.1 Uniform Flow

The first incompressible flow that we will consider is the uniform flow. Consider a flow with a uniform free-stream velocity V_∞ that is oriented in the positive x direction, shown in Fig.3(a). This uniform flow can be defined with the potential function [3]

$$\phi = V_\infty r \cos(\theta) \tag{7}$$

Note that we are using a polar coordinate system, which will simplify calculations once more complicated flows are superimposed. The resulting stream function for this flow is

$$\Psi = V_\infty r \sin(\theta) \tag{8}$$

This simple flow satisfies the mathematical conditions for incompressible, irrotational flow given by Laplace's equation. Moreover, the streamlines and equipotential curves are perpendicular, which can be confirmed by Eqs. 7 and 8. These conditions will apply to every flow we consider.

4.1.2 Source and Sink Flow

Consider a flow where all the streamlines are straight lines converging or diverging from a central point O. If the flow is converging to the central point, the flow is referred to as a sink flow. Conversely, if the flow is diverging from the central point, the flow is referred to as a source flow. The resulting velocity field for these flows only has a radial component V_r, which is inversely proportional to the distance from O. With these boundary conditions in place, the potential and stream functions for a source and sink are given as [3]

$$\phi = \frac{\Lambda}{2\pi} \ln(r) \tag{9}$$

$$\Psi = \frac{\Lambda}{2\pi} \theta \tag{10}$$

Where Λ is the source strength, which is the rate of volume flow from the source, and r is the distance from O. A positive Λ value refers to a source, whereas a negative Λ value

refers to a sink. A source or sink flow satisfies Eq. 1 at every point except for the origin, at which the divergence is infinite. The origin is thus considered a singular point. A diagram of a source and sink flow is shown in Fig. 4(a).

4.1.3 Superposition of Doublet Flow

The source and sink flow can be superimposed to create an important flow known as the doublet flow. Consider a source and sink flow of strength Λ separated by a distance $2d$. As d approaches 0, a doublet flow is formed, with a flow pattern shown in Fig. 4(b). The velocity potential and stream function are given by the equations [3]

$$\phi = \frac{\kappa}{2\pi}\frac{\cos(\theta)}{r} \tag{11}$$

$$\Psi = -\frac{\kappa}{2\pi}\frac{\sin(\theta)}{r} \tag{12}$$

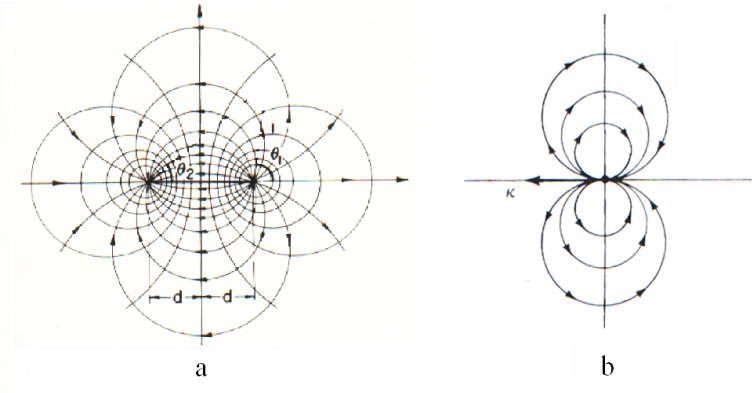

Figure 4: *(a) A source/sink flow combination* [4]. *The source and sink are separated by a distance 2d. (b) As d approaches zero, a doublet flow is formed.* [3]

Where κ is the doublet strength. The superposition of the doublet and uniform flows provides a model for the flow around a cylinder. Adding the potential functions given by Eqs. 7 and 11 yields

$$\phi = V_\infty r \cos(\theta) + \frac{\kappa}{2\pi} \frac{\cos(\theta)}{r} \tag{13}$$

Note that this superposition of flows is justified by the linear nature of Laplace's equation. A plot of the resulting streamlines from the flow superposition is shown in Fig. 5(a). Note that setting $\Psi = 0$ yields a circle of radius R, given by

$$R = \sqrt{\frac{\kappa}{2\pi V_\infty}} \tag{14}$$

The resulting flow external to R is a valid model of the incompressible, irrotational flow around a cylinder. However, the entire flow field is symmetrical about the horizontal axis, meaning that this flow generates no lift on the cylinder. To model a lifting flow, a vortex flow must be superimposed.

4.1.4 Adding Circulation with Vortex Flow

The vortex flow is defined as a flow where all streamlines are concentric circles about a given point O. The tangential velocity V_θ is inversely proportional to the distance from O. The resulting velocity potential of the vortex flow is given by the equation [3]

$$\phi = -\frac{\Gamma\theta}{2\pi} \tag{15}$$

Where Γ is the strength of the vortex flow, which is also referred to as the circulation. The superposition of the doublet, uniform, and vortex flows yields a potential function and a stream function by

$$\phi = V_\infty r \cos(\theta) - \frac{\Gamma}{2\pi}\theta + \frac{\kappa}{2\pi} \frac{\cos(\theta)}{r} \tag{16}$$

$$\Psi = V_\infty r \sin(\theta) + \frac{\Gamma}{2\pi} \ln(r) - \frac{\kappa}{2\pi} \frac{\sin(\theta)}{r} \tag{17}$$

The streamlines for this final superposition of three flows is shown in Fig. 5(b). Because there is a vortex flow, the cylinder is now rotating with a finite angular velocity. This rotation eliminates the symmetry along the horizontal axis, creating an uneven pressure distribution, which generates lift. Eqs. 16 and 17 therefore are solutions to the lifting flow around a rotating cylinder.

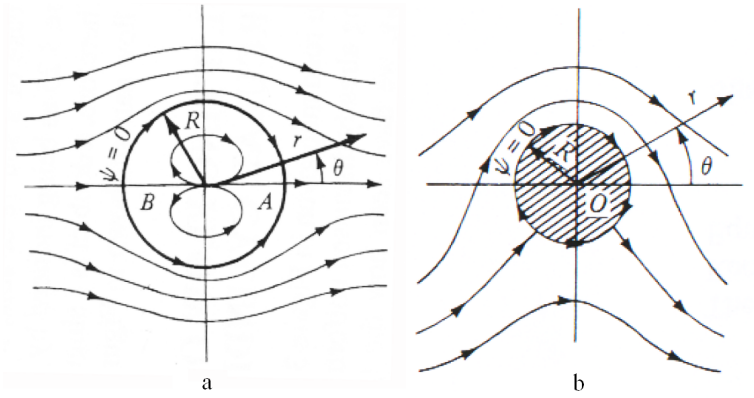

Figure 5: *(a) Non-lifting flow over a cylinder formed by synthesis of doublet and uniform flows. (b) Lifting flow over a cylinder formed by synthesis of doublet, uniform, and vortex flows.* [3]

4.2 The Lift Around a Rotating Cylinder

Once the flow around a rotating cylinder has been solved for, the lift can be computed by means of the Kutta-Joukowski theorem. This fundamental theorem of aerodynamics relates the lift per unit span on an airfoil to the speed V_∞ of the airfoil through the fluid, the fluid density ρ, and the circulation Γ. When Γ is known, the lift per unit span L' becomes

$$L' = \rho V_\infty \Gamma \tag{18}$$

The definition of Γ as shown in Eq. 18 is the line integral of the velocity field over the closed curve of the airfoil. Circulation is a conceptual tool that relates the lift on an object to the nature of the fluid flow around it. Specifically, circulation is related to vorticity on any open surface bounded by the airfoil curve using Stokes' theorem

$$\Gamma = \oint \vec{V} \cdot d\vec{s} = \iint (\nabla \times \vec{V}) \cdot d\vec{S} = \iint \vec{\omega} \cdot d\vec{S} \tag{19}$$

For the lifting flow around a cylinder, the only source of vorticity comes from the vortex flow, which has an infinite vorticity at the origin but zero vorticity at every other point. This point source of vorticity leads to the finite circulation Γ. However, recall that Γ is also the strength of a vortex flow, as defined in Eq. 15. Therefore, for a flow given by Eq. 16, there are an infinite number of arbitrary Γ values, each corresponding to a different flow solution satisfying Eq. 4. The Γ value corresponding to the physically correct inviscid flow solution for a specific cylinder must therefore be determined by applying the Kutta condition.

As mentioned earlier, the Kutta condition defines Γ as the value that creates stagnation points at the x intercepts A and B of the cylinder in the z plane, as shown in Fig. 7(a) and (b). At the cylinder's boundary, there can only be a velocity component in the θ direction because by definition, no flow can emerge from the cylinder. The velocity component in the θ direction is given by [16]

$$V_\theta = -(2V_\infty \sin(\theta) + \frac{\Gamma}{2\pi R}) \tag{20}$$

Where R is the radius of the cylinder. The Kutta condition defines the velocity component at an angle of β and -β to be 0, where β is the angle between the x axis and the line segment from the x-intercept to the cylinder center, as shown in Fig. 7(b). Plugging β into Eq. 20, setting V_θ=0, and solving for Γ yields

$$\Gamma = 4\pi V_\infty R \sin(\beta + \alpha) \tag{21}$$

Where α is the angle of the freestream velocity with respect to the x axis. Eq. 21 allows for computation of the correct circulation value for a given cylinder in a given free stream.

4.3 Mapping from a Cylinder to an Airfoil with the Joukowsky Transformation

Having solved for the flow around a cylinder with the superposition of three elementary flows, we need to relate this solution to an airfoil shape. To accomplish this, we use a conformal mapping function called the Joukowsky transformation. The Joukowsky transformation is used because it has the property of transforming circles in the z plane into shapes that resemble airfoils in the w plane [5]. Figure 6(a) shows a circle in the z plane defined by the equation

$$z = be^{i\theta} \tag{22}$$

Where b is the radius of the circle and θ ranges from 0 to 2π. The Joukowsky transformation is given by the function [16]

$$w(z) = z + \frac{\lambda^2}{z} \tag{23}$$

Where w is the function in the transformed plane, and λ is the transformation parameter that determines the resulting shape of the transformed function. For $\lambda = b$, the circle is mapped into a flat plate going from -2b to 2b, as shown in Fig. 6(b). On the other hand, setting the transformation parameter λ larger than b causes the circle to be mapped into an ellipse, as shown in Fig. 6(c).

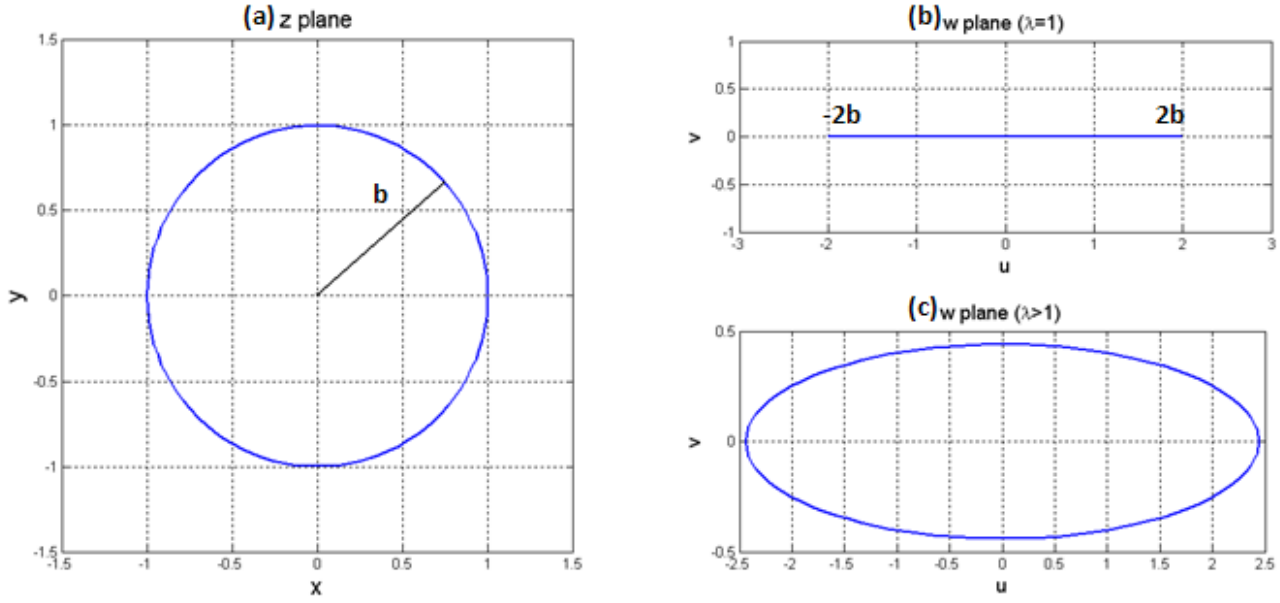

Figure 6: *(a)A circle in the z plane with radius b=1 and center at the origin is transformed to the w plane using the Joukowsky Transform. (b) For λ=1, the circle is transformed into a flat plate of length 4b. (c) For λ > 1, the circle is transformed into an ellipse.*

.

However, neither of the shapes in Fig. 6 resemble an airfoil. The airfoil shape is realized by creating a circle in the z plane with a center that is offset from the origin, as shown in Fig. 7(a). If the circle in the z plane is offset slightly, the desired transformation parameter is given as [16]

$$\lambda = b - |s| \tag{24}$$

Where s is the coordinates of the center of the circle. The transformation in the w plane resembles the shape of an uncambered airfoil symmetric about the x axis, as shown in Fig. 7(c). The x coordinate of the circle origin therefore determines the thickness distribution of the transformed airfoil.

If the center of the circle in the z plane is also offset on the y axis, the Joukowsky transformation yields an unsymmetrical, cambered airfoil as shown in Fig. 7(d). This shows

that the y coordinate of the circle center determines the curvature of the transformed airfoil.

The airfoil shapes created from the Joukowsky transformation are known as Joukowsky airfoils. The x intercepts of the circle in the z plane become the leading and trailing edges of the mapped airfoil in the w plane [5]. Fig. 7 also shows that the Joukowsky airfoil has a cusp at the trailing edge, which is a mathematical property that is not present in real airfoil shapes [12].

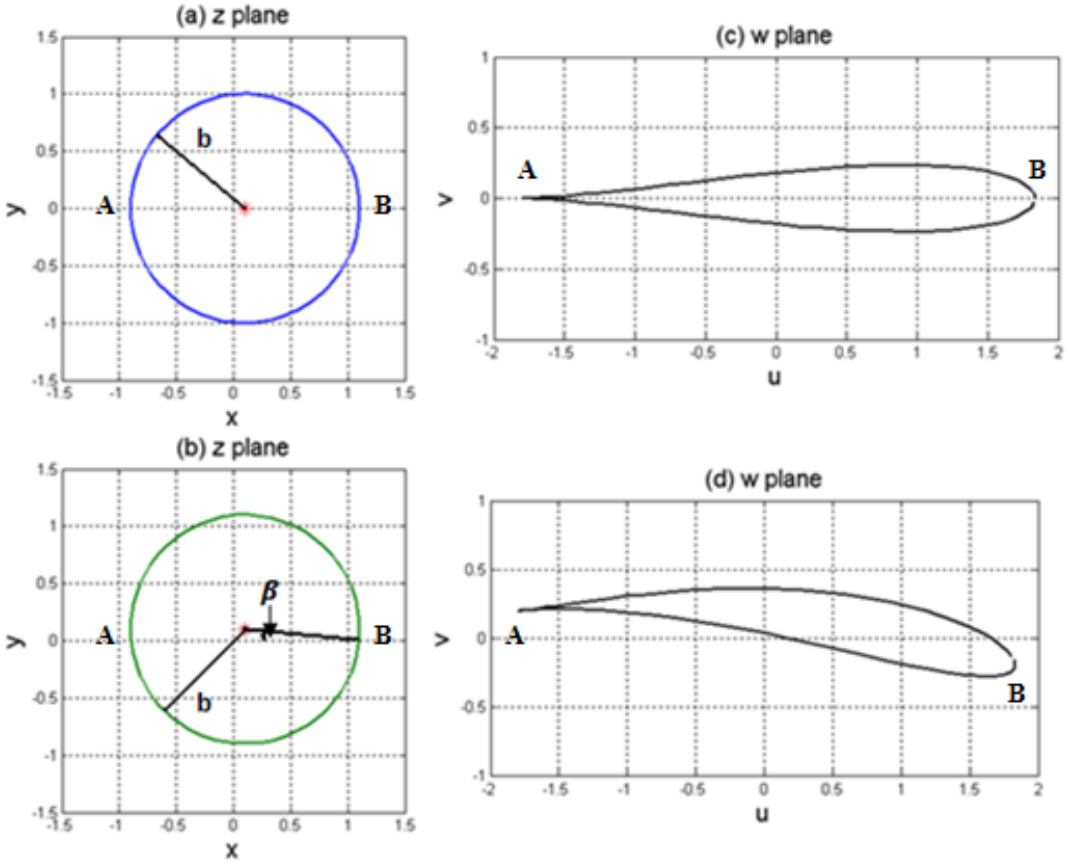

Figure 7: *(a) Cylinder in z plane with center offset on the x axis. (b) Cylinder in z plane with center offset on x and y axis. (c) Joukowsky Transform of cylinder in (a) with* $\lambda = b - |s|$. *The transform results in a noncambered airfoil in w. (d) Joukowsky Transform of cylinder in (b) with* $\lambda = b - |s|$. *Transform results in a cambered airfoil. In both (c) and (d) A and B are stagnation points corresponding to the x-intercepts of the cylinders in (a) and (b).*

.

In addition to the circle in the z plane being transformed, the flow around the circle

can also be transformed because of the previously mentioned angle preserving feature of conformal mapping functions. This requires that the velocity potential and stream function given in Eqs. 16 and 17 be expressed as a complex function, just as the airfoil shape must also be defined using complex variables. This is accomplished by expressing the velocity potential and stream function in a complex potential, given by [4]

$$w(z) = \phi + i\Psi \tag{25}$$

Thus, the flow past a cylinder can be written with the complex potential [16]

$$w(z) = V_\infty(z + \frac{R^2}{z}) + i(\frac{\Gamma}{2\pi}\ln(z)) \tag{26}$$

Because the flow solution can be transformed in the w plane, the circulation Γ derived in Eq. 21 for a cylinder is the same as the circulation for the transformed airfoil. Because of this, L' calculated in Eq. 18 for a circle in the z plane is the same L' for the transformed airfoil in the w plane.

5 Simulation Results and Analysis

With the solution for the lifting flow around a cylinder and a method for converting this solution into the flow around a Joukowsky airfoil, computational tools can be used to visualize this flow and develop lift calculations for several real airfoils.

5.1 Computing the Streamlines around an Airfoil

The Joukowsky airfoil can be visualized by having a computational graphing program apply the Joukowsky transform to an offset circle. The flow about this airfoil can be plotted by generating a contour plot of the imaginary component of the complex potential given in Eq.

26, which corresponds to the stream function of the flow. Fig. 8(a) shows the streamlines of flow around a cylinder. Fig. 8(b) shows streamlines of flow about the corresponding transformed Joukowsky airfoil at an angle of attack of 0 degrees.

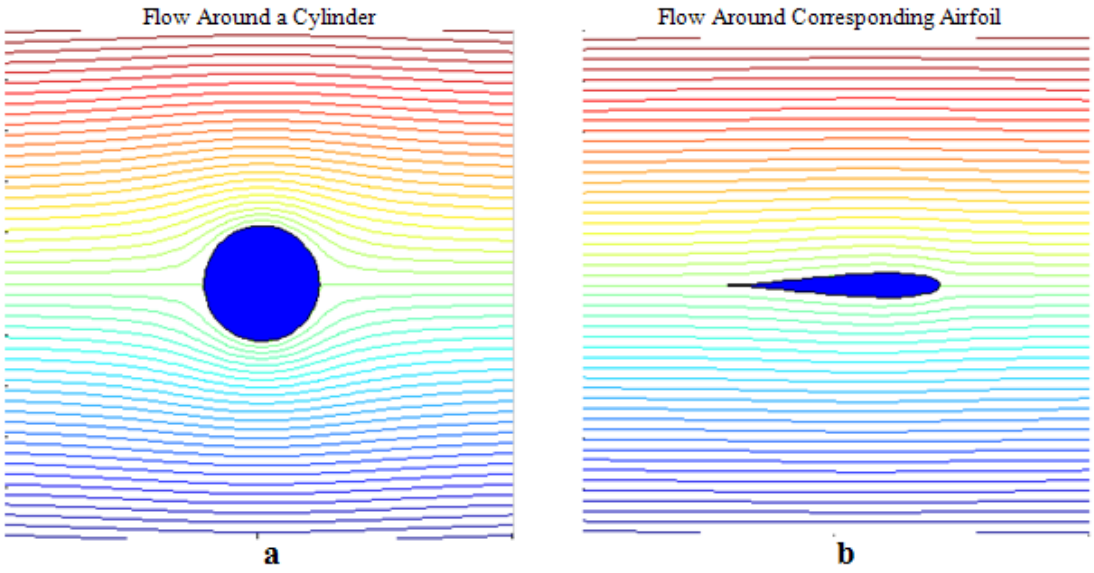

Figure 8: *Computer generated plot of (a) streamlines around cylinder in z plane and (b) corresponding Joukowsky airfoil. The plot was generated with* V_∞*=100 m/s,* α*=0, and* ρ*=1.225* kg/m^3*. No lift is generated on the cylinder or the airfoil because of the symmetric fluid flow. The figure shows streamlines meeting at the trailing edge of the airfoil, indicating the Kutta condition is satisfied. The cylinder parameters used were* $x = .1$ *m,* $y = 0$ *m,* $r = 1.13$ *m. Solution plotting algorithm was derived with help from* [6]

.

The flow around the cylinder and the airfoil can be validated qualitatively. Since α is zero, we expect there to be a symmetric distribution of streamlines about the x axis. This appears in both the flows for the airfoil and the circle. We also expect the streamlines to flow around the leading edge of the cylinder and airfoil and meet smoothly at the trailing edge.

5.2 Computation of Lift around NACA Airfoils

One of the potential applications of Joukowsky airfoils is that we can use them to model the lift around NACA airfoils. However, this requires a method of matching transformed Joukowsky airfoils to the NACA airfoils we wish to model. This method is needed because the Joukowsky transform only maps a circle into an airfoil. Ideally, an inverse Joukowsky transform could be used to map a desired airfoil shape into a simpler circular geometry, but this method requires the use of branch cuts [4], a complex variables concept that is beyond the scope of this paper.

Instead, we used a simpler "trial and error" method to determine the circles that would produce airfoils most identical to the NACA airfoils we wished to model. We analyzed three NACA airfoils: the NACA 0012, the NACA 2215, and the NACA 4412. These airfoils were chosen because they are commonly used in airplane applications and have been well studied. We first plotted each of these NACA airfoils, and then made an initial guess for a circle that would transform into an airfoil that would resemble each NACA cross-section. We obtained this initial guess from a similar Joukowsky transformation program offered by NASA [11]. We then modified the radius and center of the circle until the corresponding Joukowsky airfoil visually matched the NACA airfoil. The final circle properties we arrived at for each NACA airfoil are displayed in Table 1.

Table 1: Cylinder parameters used to generate Joukowsky airfoils

Airfoil Height	**X Value (m)**	**Y value(m)**	**Radius(m)**
NACA 0012	-.107	0	1.027
NACA 2215	-.130	.01	1.110
NACA 4412	-.100	.06	1.130

In order to first plot the NACA airfoils, we used a set of quartic equations that plot the upper and lower surfaces of the airfoil from the 3 properties given in a NACA 4-series

airfoil. Analysis of these equations is not presented in this paper, but for these equations the reader is referred to an external resource [1]. Plots of these NACA airfoils and the Joukowsky airfoils we used to model them are shown in Fig 9. To confirm the validity of these Joukowsky airfoils beyond a visual estimate, we performed a quantitative analysis to determine the relative error in our model. This will be presented in the next section.

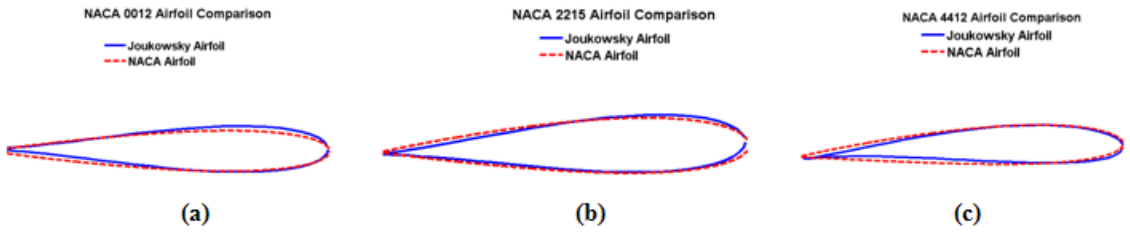

Figure 9: *Comparisons between: (a) actual NACA 0012 Airfoil and Joukowsky model of NACA 0012 airfoil (b) actual NACA 2215 Airfoil and Joukowsky model of NACA 2215 airfoil (c) actual NACA 4412 Airfoil and Joukowsky model of NACA 4412 airfoil*

.

As Fig. 9 shows, the shapes of the Joukowsky airfoils do not match the shapes of the NACA airfoils perfectly. We found that it was difficult to develop Joukowsky airfoils that exactly match the NACA airfoils. The biggest reason for this is that Joukowsky airfoils are an idealized mathematical shape, as mentioned earlier. The trailing edge of every Joukowsky airfoil must end in a cusp because of the nature of the Joukowsky transformation, whereas NACA airfoils have finite trailing edge angles. This cusp requirement means that the Joukowsky airfoil will converge at the trailing edge more rapidly than the corresponding NACA airfoil.

Once we found Joukowsky airfoils that closely matched the NACA airfoils, we computed the lift coefficient L_c on each airfoil as a function of the angle of attack α using the Kutta-Joukowsky theorem from Eq. 18 and the circulation equation from Eq. 21. We found lift coefficients at angles of attack ranging from 0 degrees to 12 degrees. The lift coefficient is a nondimensional coefficient that relates the lift generated by an airfoil, the dynamic pressure

of the fluid flow around the airfoil, and the area of the airfoil. The lift coefficient is given by the equation [16]

$$L_c = \frac{\Gamma}{2V_\infty^2 b} \tag{27}$$

Because the lift coefficient factors in the dynamic pressure and the size of the airfoil, L_c thus depends only on the shape of the airfoil and the angle of attack. Figs. 10 to 13 show plots of the lift coefficient for each airfoil as a function of α. The data from our simulation is plotted against a curve showing lift coefficients found using thin airfoil theory, an alternate method of modeling lift on an airfoil. Thin airfoil theory models the flow around an airfoil by treating the airfoil as a distribution of vortices along the mean camber line. This method still relies on potential flow theory and thus utilizes the same incompressible, inviscid fluid assumptions as our Joukowsky airfoil model. Therefore, as long as the thickness of the airfoil is small compared to its chord length, lift coefficients found using the the thin airfoil method provide a valid comparison point to lift coefficients found from Joukowsky airfoils. The results obtained from thin airfoil theory can be assumed to reasonably predict the linear portion of the relationship between the angle of attack of a real airfoil and the lift it generates in a low speed flow [14]. Thin airfoil lift coefficients were determined by means of an externally developed computational simulation [9]. For further information on thin airfoil theory, the reader is referred to an external resource [8].

Fig. 10 shows the predicted lift curve for the NACA 0012 airfoil. The lift curve shows that there is no lift generated at an angle of attack of 0 degrees. This is expected because the NACA 0012 is an uncambered airfoil and is thus symmetric about the chord. When $\alpha = 0$, the flow about the airfoil is symmetric, and no lift is generated. Secondly, Fig. 10 also shows that the lift increases proportionally with the angle of attack. This linear relationship between lift coefficient and angle of attack is an important aerodynamic characteristic of

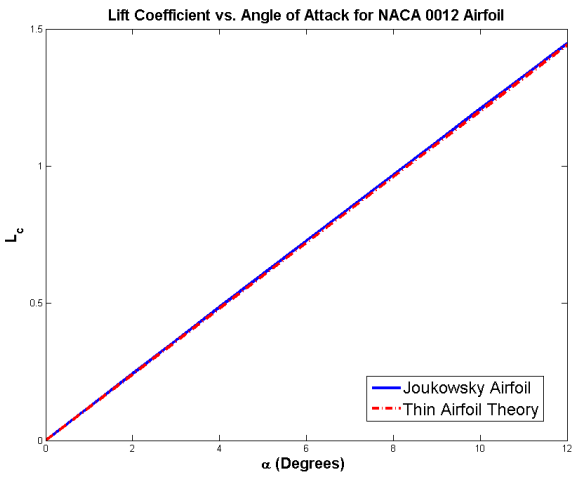

Figure 10: *Dependence of lift coefficient on angle of attack for NACA 0012 airfoil at $V_\infty = 100$ m/s, $\rho = 1.225$ kg/m^3. The airfoil generates no lift at a zero angle of attack due to the symmetry of the NACA 0012 design. The lift data from the Joukowsky airfoil matches the lift data obtained from the thin airfoil method very precisely.*

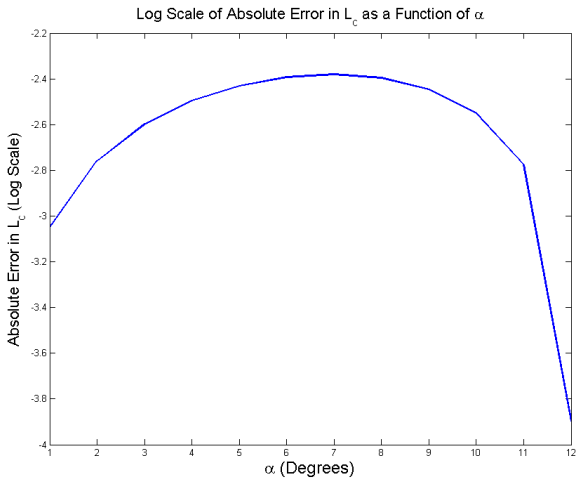

Figure 11: *Absolute value of difference in lift coefficients for Joukowsky Airfoil and actual NACA 0012 airfoil. Differences are shown on a log scale. The results indicate the lift coefficients are in agreement to within 2-4 decimal places.*

airfoils. The lift curve predicted from our Joukowsky airfoil matches the lift curve predicted using the thin airfoil method very well. Fig. 11 shows the absolute value of the error in lift curve data on a log scale as a function of α. The plot indicates that the two lift curves are generally equivalent to within 2-4 decimal places.

Figures 12 and 13 show the aerodynamic performance of the NACA 2215 and 4412 airfoils, respectively. Since both airfoils are nonsymmetric about the x axis due to their cambered shape, we would expect them both to have nonzero lift coefficients at a zero angle of attack. Both airfoils satisfy this requirement, and furthermore, both airfoils have the same linear response that was observed for the NACA 0012 airfoil. Unfortunately, the lift curves predicted using our Joukowsky airfoil model do not match up as well with the results from the thin airfoil method. Both airfoils seem to under-approximate the lift coefficient,

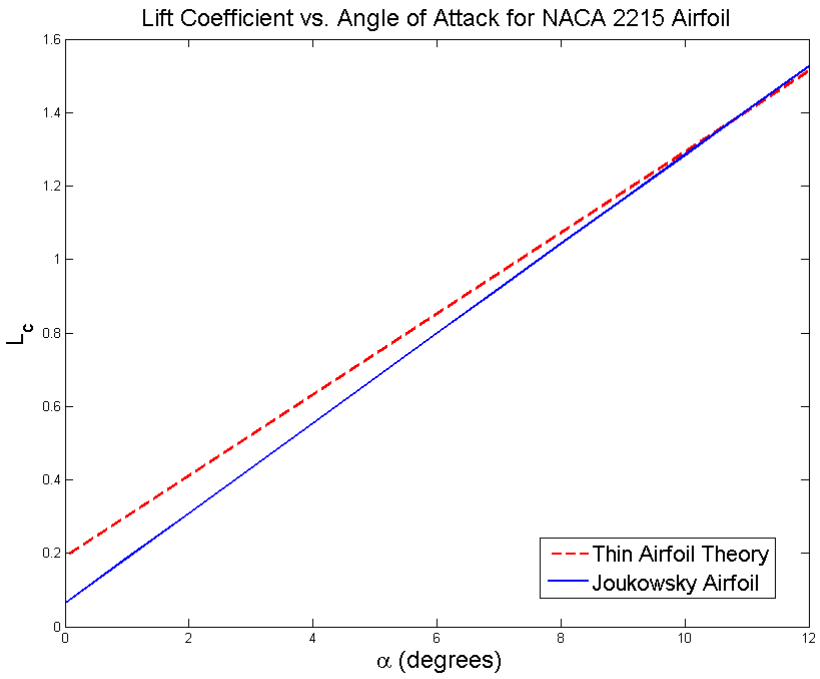

Figure 12: *Dependence of lift coefficient on angle of attack for NACA 2215 airfoil at* V_∞ *= 100 m/s,* ρ *= 1.225 kg/m*^{3}*. The lift data from the Joukowsky airfoil has a significant discrepancy with the lift data obtained from the thin airfoil method at lower angles of attack, although the data from the two models matches up better as the angle of attack increases.*

especially at lower values of α. As α increases, the results from our model match up better with the results from the thin airfoil method.

It is important to keep in mind that the linear response of L_c with increasing α is only realistically valid over a certain range. As the angle of attack increases towards the stall angle, the lift coefficient suddenly reaches a peak and then drops off rapidly. As mentioned earlier, this occurs because the fluid flow around an airfoil no longer meets smoothly at the trailing edge [3]. Mathematically, we interpret this to mean that the Kutta condition is no longer applicable, and neither our model nor the thin airfoil method can be used to predict the lift coefficient. While the exact value of the stall angle depends on a number of factors, we are modeling the lift coefficient at angles of attack well below the stall angle for all three airfoils.

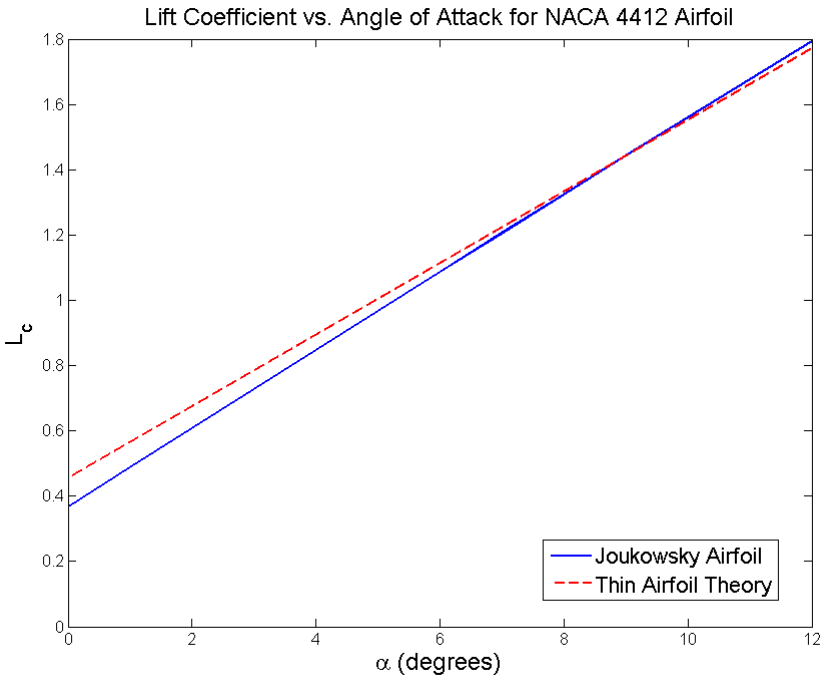

Figure 13: *Dependence of lift coefficient on angle of attack for NACA 4412 airfoil at* $V_\infty = 100\ m/s$, $\rho = 1.225\ kg/m^3$. *The lift data from the Joukowsky airfoil has a small discrepancy with the lift data obtained from the thin airfoil method at lower angles of attack, but this discrepancy decreases as the angle of attack increases.*

6 Error Analysis

6.1 Overview

Given that we initially used a visual trial and error method to compare our transformed Joukowsky airfoils to the NACA airfoils, it is important to perform a quantitative error analysis to analyze discrepancies in our model. However, there is an important observation we can make without a specific quantitative analysis. The lift curves from the Joukowsky airfoil matched up better with the lift curves obtained from thin airfoil calculations when an uncambered airfoil was analyzed compared to the two cambered airfoils. This indicates that discrepancies are larger when the airfoil has a non-symmetric geometry, and that inaccuracies associated with our method are more apparent when modeling airfoils with a curved shape.

6.2 Method of Error Analysis

Our primary form of error analysis was to compare properties of the NACA airfoils with those of the Joukowsky airfoils. We determined that the two most important properties to compare would be the area and perimeter of each airfoil. The area of each airfoil was found using a trapezoidal approximation of the absolute value of the area enclosed by each airfoil. To determine the perimeters of the NACA airfoils, we computed the arc length of the upper and lower airfoil surfaces using the arc length formula for a single valued function [13]. The perimeters of the Joukowsky airfoils were computed by using the arc length formula for a parametric equation [13]. The integration in the arc length formula was also evaluated numerically using a trapezoidal approximation.

6.3 Error Analysis Results

Table 2 shows the results obtained from the perimeter and area calculations. The table shows that the Joukowsky airfoils and the NACA airfoils have areas that are similar, but perimeters that are different. Interestingly, the relative error between the actual NACA airfoil perimeter and the Joukowsky airfoil perimeter is similar for each airfoil, around 20-30%. This discrepancy in perimeter is due to the cusp in the Joukowsky airfoil, which causes a more curved airfoil shape that increases the perimeter without increasing the enclosed area significantly.

Unfortunately, the results in Table 2 do not provide a clear explanation for the discrepancy in some of the lift curves. The NACA 0012 airfoil has a discrepancy in perimeter between the actual airfoil and the Joukowsky airfoil, yet the lift curve for the Joukowsky airfoil matches the results seen using thin airfoil theory. On the other hand, the Joukowsky airfoils for the NACA 2215 and 4412 have both a discrepancy in the airfoil perimeter and a discrepancy in the lift curve results. Thus, the effect of perimeter on the aerodynamic

Table 2: Discrepancies between Joukowsky airfoil shapes and actual NACA airfoil shapes

Airfoil Type	**Property**	**Joukowsky Airfoil**	**Actual Airfoil**	**Relative Error** (%)
NACA 0012	Perimeter(m)	11.7914	9.1521	28.8
	Area (m^2)	1.7184	1.6944	1.40
	Perimeter/Area	6.8618	5.4014	27.0
NACA 2215	Perimeter(m)	11.9729	9.7215	23.2
	Area (m^2)	2.3242	2.3665	1.80
	Perimeter/Area	5.1514	4.1079	25.4
NACA 4412	Perimeter(m)	12.0025	9.9500	20.6
	Area (m^2)	1.7608	1.9944	11.7
	Perimeter/Area	6.8165	4.9890	36.6

performance is also unclear. It would appear that an airfoil with a larger perimeter would maximize the circulation line integral seen in Eq. 19, and thus increase the lift. However, the Joukowsky airfoils have a larger perimeter, but lower lift coefficients.

The error analysis shows that a comparison of the perimeter and area of the airfoils does not shed light on the lift discrepancies seen in the last section. However, we can use the results from Table 2 to develop an estimate of how much relative error to expect in our model. To determine this relative error boundary, we divided the airfoil perimeter by the area to obtain a final comparison parameter. We then computed the error in this parameter for each Joukowsky airfoil. From this we concluded that the expected relative error in the NACA 0012 airfoil is 27%, while the relative errors in the NACA 2215 and 4412 airfoils are 25% and 37%, respectively. Looking at the lift coefficient values in Figs. 10 and 13, our results for the NACA 0012 and 4412 airfoils fall within this error boundary. However, the maximum error in the lift coefficient values for the NACA 2215 airfoil exceeds the predicted relative error calculated in Table 2.

7 Conclusion

The overall goal of our analysis was to effectively model the fluid flow around airfoils using the conformal mapping technique. We were able to successfully map the solution for the inviscid flow around a cylinder to the flow around an airfoil shape using the Joukowsky transformation. However, we had more varied results with our attempt to model the lift around NACA airfoils. This variation was likely the result of differences in the shapes between the NACA airfoils and the Joukowsky airfoils, particularly at the trailing edge. While the NACA 0012 was modeled successfully with our Joukowsky airfoil model, there were discrepancies between our data and the thin airfoil data for the NACA 2215 and 4412 airfoils, particularly at low angles of attack.

Further analysis in this field should focus on determining the exact cause of this error. An analysis of the airfoil perimeter and area for both airfoil types demonstrated that neither of these properties were directly responsible for the error observed in the lift modeling. However, an analysis of other geometric differences, such as the cusp in Joukowsky airfoils, could uncover the reason behind the error. Another potential area of analysis is conformal mapping with a more complicated transformation function, such as the Karman-Trefftz transform, which accounts for the finite angle at the trailing edge of NACA airfoils.

References

[1] Alexander, Greg. *NACA Airfoil Series.* Aerospaceweb.org. http://www.aerospaceweb.org/question/airfoils/q0041.shtml.

[2] Anderson, David and Scott Eberhardt. *Understanding Flight.* 2nd Edition. Prentice Hall, 1988.

[3] Anderson, John D. *Fundamentals of Aerodynamics*. 4th Edition. New York: McGraw-Hill, 2007.

[4] Bear, Jacob. *Dynamics of Fluids in Porous Media*. Canada: American Elsevier, 1972.

[5] Benson, Thomas J. *Interactive Educational Tool for Classical Airfoil Theory*. Cleveland, Ohio: NASA Lewis Research Center, Oct. 30, 1996. http://www.grc.nasa.gov/WWW/K-12/airplane/FoilTheory.pdf.

[6] Isola, Dario. *Joukowski Airfoil Transformation*. MATLAB Central. http://www.mathworks.com/matlabcentral/fileexchange/loadFile.do?object Id=8870.

[7] Katz, Joseph and Allen Plotkin. *Low Speed Aerodynamics*. 2nd Edition. New York: McGraw-Hill, 1991.

[8] Kroo, Ilan. *Applied Aerodynamics: A Digital Textbook*. http://www.desktopaero.com/appliedaero/preface/preface.html

[9] Marchman, Dr. James F. *Computer Programs for AOE 3014*. Virginia Polytechnic: Aerospace and Ocean Engineering Department. http://www.aoe.vt.edu/ marchman/software/.

[10] Matthews, John H. and Russell W. Howell. *Dictionary of Conformal Mapping: Part 1*. California State University Fullerton, 2008. http://math.fullerton.edu/mathews/c2003/ConformalMapDictionary.1.html.

[11] National Aeronautics and Space Administration. *Conformal Mapping: Joukowski Transformation*. http://www.grc.nasa.gov/WWW/K-12/airplane/map.html

[12] Panton, Ronald L. *Incompressible Flow: Third Edition*. Van Dyke: Cambridge University Press, 1996.

[13] Stewart, James. *Multivariable Calculus: Sixth Edition*. Brooks Cole, 2007.

[14] Scott, Jeffrey A. *Lift Coefficient and Thin Airfoil Theory.* http://www.aerospaceweb.org/question/aerodynamics/q0136.shtml

[15] U.S. Centennial of Flight Commission. *Airfoil Diagram.* www.centennialofflight.gov/essay/Dictionary/angleofattack/DI5.htm

[16] Walsh, Paul. *Introduction to Conformal Mapping in Aerodynamics*. Dept. of Aerospace Engineering, Ryerson University. www.ryerson.ca/ p3walsh/aer504/conformal.doc.